Behavior and Limit States of Long-Span Composite Floor Beams with Simple Shear Connections subject to Compartment Fires: Experimental Evaluation

Lisa Choe, M. ASCE[1]; Selvarajah Ramesh, A.M. ASCE[2]; William Grosshandler[3]; Matthew Hoehler, M. ASCE[4]; Mina Seif, M. ASCE[5]; John Gross, F. ASCE[6]; Matthew Bundy[7]

Abstract:

This paper presents the results of compartment fire experiments on four 12.8 m long composite floor beams with various end support conditions. Specimens were constructed as partially-composite beams, consisting of W18×35 steel beams and 83 mm thick lightweight concrete slabs cast on top of 76 mm deep ribbed steel deck units. Test variables included two types of simple shear connections (shear-tab and welded-bolted double-angle connections) and the presence or absence of slab continuity over the girders. Each specimen was subjected to gravity loading using hydraulic actuators and 4000 kW compartment fires produced using natural gas-fueled burners. This study evaluated the characteristics of the fire loading and thermal and structural responses of the specimens. The test results indicated that there were significant effects of thermal restraints on the behavior and failure modes of the specimens with simple shear connections. The specimens resisted gravity loads at large vertical displacements near midspan (approximately a ratio of span length over 20) without collapse under fire loading. However, various limit states and vulnerabilities to fires were observed, including local buckling of steel beams near supports, flexural failure (yielding of steel beams and concrete fracture near restrained end supports), and

[1] Research Structural Engineer, National Institute of Standards and Technology, Gaithersburg, MD 20899-8666 (corresponding author) E-mail:lisa.choe@nist.gov
[2] Guest Researcher, National Institute of Standards and Technology, Gaithersburg, MD 20899.
[3] Guest Researcher, National Institute of Standards and Technology, Gaithersburg, MD 20899.
[4] Research Structural Engineer, National Institute of Standards and Technology, Gaithersburg, MD 20899.
[5] Guest Researcher, National Institute of Standards and Technology, Gaithersburg, MD 20899.
[6] Guest Researcher, National Institute of Standards and Technology, Gaithersburg, MD 20899.
[7] Supervisory Mechanical Engineer, National Institute of Standards and Technology, Gaithersburg, MD 20899.

connection failure (weld shear or bolt shear) during heating and cooling which could lead to partial or total collapse of the floor system.

Authors Keywords: Fire; Composite beam; Floor slab; Connection; Experimental testing; Failure

Introduction and Background

Composite beams supported by simple shear connections are a standard type of floor framing construction for multi-story steel buildings because of their cost-effectiveness in spanning large open spaces. Composite beams consist of concrete slabs cast on formed steel decks connected to steel beams using steel headed stud anchors. The composite action between floor beams and concrete slabs increases the stiffness of the floor system, allowing longer spans and lighter beams than found in non-composite construction. A typical length of composite beams used in commercial buildings ranges from 12 m to 15 m (SCI 2008).

When exposed to fires, however, the behavior of long-span composite beams becomes complex and difficult to predict using conventional design equations and methods for loading conditions at ambient temperatures. Temperatures of composite beams vary through the section depth and change with the duration of fire exposure, thereby developing thermal gradients. Composite interaction, characterized by the slip capacity of shear connections between concrete slabs and steel beams, depends on the temperature distribution and applied loads. Furthermore, thermal strains developed in long-span composite beams can introduce large forces and displacements which vary greatly depending on the stiffness of the support frames and connections. Some beam end connections can be vulnerable to the effects of the thermal restraint to elongation and contraction of fire-exposed long-span beams (NIST 2008). Failure of steel connections could trigger a partial or total collapse of a building.

In current design practice, the structural integrity of composite floor assemblies in fires relies heavily on passive fire protection systems prescribed in national building codes, e.g., the *International*

Building Code (IBC) (ICC 2018) and the *Building Construction and Safety Code* (NFPA 2018). Sprayed Fire-Resistive Materials (SFRM) are the most common materials applied to exposed steel substrates of structural members and assemblies to achieve prescribed fire-resistance ratings. Adequacy of insulating materials and associated installation details must be certified by standard fire testing, e.g., ASTM E119 (2018). The fire-resistance ratings, expressed in hours, for composite beams and floor assemblies installed with commercial insulation products can be found, e.g., in the Underwriters Laboratory fire-resistance directory. However, the limiting criteria achieved during standard fire tests and structural responses of specimens (forces and displacements) generally remain as proprietary information (ASCE 2018).

Previous experimental studies on isolated composite beams (Wainman and Kirby 1987; Newman and Lawson 1991; Zhao and Kruppa 1997; Alfawakhiri et al. 2016) have focused on behavior resulting from standard fire exposure. The span length of specimens seldom exceeded 6 m due to size limitations of furnaces, and the beam end supports employed did not fully capture important characteristic behavior of composite steel frames, such as redistribution of forces. Rather, the ends of specimens were either simply supported allowing free thermal expansion and rotation or fully fixed at the reaction frames.

Very few experimental studies have been conducted on composite beams supported by simple shear connections under fire loading. The first Cardington test in 1995 (Kirby 1998) was conducted on the 9 m long unprotected composite beam framed into the 7th floor of an 8-story prototype building. A gravity load of 5.5 kN/m^2 was applied using sand bags, and thermal loading (3°C/min to 10°C/min) was applied using a gas furnace. The beam ends and the flexible end-plate connections to columns were kept outside the furnace. Test results indicated that local buckling occurred at the ends of the steel beam inside the furnace because of the restraint to thermal elongation, followed by large vertical displacements at midspan (approximately a ratio of the beam span over 40). Failure of connections occurred at one end during cool-down but did not result in collapse of the composite floor.

More recently, researchers in the United States have tested mechanically-loaded composite beams with simple shear connections at elevated temperatures. Selden et al. (2016) tested five partially-composite beams with flat concrete slabs subjected to thermal loading using ceramic radiant heaters. The beam span was 3.8 m, and various types of simple shear connections supported composite beams, including single-plate (shear-tab), single-angle and double-angle connections. The flexural strength of the specimens was reduced by heating effects. One of the specimens exhibited compressive failure of flat concrete slabs subjected to excessive loading at temperatures below 500°C. For the other specimens, no incipient collapse was observed even if temperature of steel beams reached 700°C, but partial tensile fracture of shear tabs occurred during cool-down. Kordosky (2017) evaluated the effectiveness of SFRM on the fire resistance of 3.3 m long composite floor assemblies exposed to a standard fire. Both the reaction frames and shear-tab connections, protected with 152 mm thick ceramic blankets, were placed inside the furnace. The floor assembly, including an unprotected steel beam, failed to resist imposed gravity loads, indicating runaway vertical displacements at 28 min; the other specimen, supported by the steel beam protected with SFRM for a 2-hour fire-resistance rating, maintained its structural integrity prescribed by building codes. Although some bolts used in the shear-tab connection fractured by shear occurred due to large tensile forces during cooling, such failures did not lead to collapse of the floor assembly.

Although these studies have provided useful insights into the fire resistance of composite beams with simple shear connections, there are limitations on the beam spans, boundary conditions of concrete slabs, and design details of composite floor construction. Aforementioned studies used shorter composite beams than those used in standard composite floor construction in the United States (in the range of 10 m to 15 m). Furthermore, lack of lateral supports around the edges of concrete slabs introduced premature failure not commonly seen in composite beams as part of floor systems. Although the Cardington test incorporated realistic continuity of composite slabs, detailing of slab reinforcement and connections was based on standard British practice.

Research Motivation, Objectives, and Significance

With recognized limitations in the prescriptive approach to design for fire, there has been a renewed interest in the United States to develop performance-based design methods since the 9/11 World Trade Center disaster (ASCE 2018). Alternative engineering approaches have been established along with guidance and design references, e.g., Appendix 4 of the American National Standards Institute/American Institute of Steel Construction (ANSI/AISC) *Specification for Structural Steel Buildings* (AISC 2016) and the American Society of Civil Engineers (ASCE) *Structural Fire Engineering* (ASCE 2018). Simple calculation methods used for composite floor systems in fire, however, merely account for strength reduction in composite beams with idealized end supports at elevated temperatures. The suggested modeling approaches still require rigorous validation against experimental data characterizing thermal restraints from surrounding frames and connections, which are not readily available. A significant need exists for experimental data providing the behavior and limit states of full-scale composite floor beam assemblies exposed to realistic fires, incorporating medium-to-long spans of floor beam assemblies commonly used in industry practice. Such information cannot be achieved by standard fire testing with furnaces.

This paper presents a series of four fire experiments conducted on 12.8 m long composite floor beams supported by simple shear connections at the National Fire Research Laboratory (Bundy et al. 2016) in the National Institute of Standards and Technology (NIST). The objective of this study was to experimentally investigate the behavior and failure mechanisms of long-span composite beam assemblies subjected to imposed gravity loading and compartment fires. The beam end supports included two types of simple shear connections (shear-tab and welded-bolted double-angle connections), and slab continuity over the girders was varied. Design and construction of the specimens followed standard U.S. practice. For thermal loading, a repeatable compartment fire was produced using fully-controlled natural gas-fueled burners with the heat energy simulating structurally significant fires in typical office buildings. The measurements included (i) the fire characteristics including heat release rates, gas temperatures, and heat fluxes, and (ii) thermal (temperatures) and structural responses (displacements, forces, and strains) of the specimens. Any noteworthy observations critical to understand the overall fire performance of the specimens were made.

The experimental results presented in this paper can be used to guide the development and validation of physics-based computational models that predict the structural responses of long-span composite beams and floor assemblies in realistic fire conditions. This research effort will provide important steps toward the improvement of performance-based building code requirements for steel buildings.

Experiment Design

Design and Construction of Specimens

The specimens used in this study were 12.8 m long composite floor beams with a 2-hour fire-resistance rating, designed following the American codes and standards. The ASCE 7 (2016) gravity load combination of 1.2×dead load plus 1.6×live load was used, including a construction live load of 0.96 kN/m^2, a superimposed dead load of 0.48 kN/m^2, and a total live load of 3.35 kN/m^2 (incorporating 2.39 kN/m^2 for office use and 0.96 kN/m^2 for partitions). Fig. 1(a) shows a cross section of the specimen, consisting of a 27.6 MPa lightweight concrete slab on 20-gauge galvanized, 76 mm deep ribbed steel decking and a W18×35 steel beam. The steel deck was oriented perpendicular to the steel beam. The thickness of the topping concrete (over the top ribs) was 83 mm. The slab width was 1.83 m, which was less than the design tributary width of 3.05 m. In fire experiments, this helped to prevent longitudinal cracks in the concrete due to the weight of the slab extended from the centerline of the beam.

The steel beam was partially-composite with the concrete slab using 19 mm diameter steel headed studs welded to the top flange at a spacing of 305 mm. Fig. 1(b) shows a single stud welded off-center in each bottom rib of the deck, representing the strong stud position according to ANSI/AISC 360 (AISC

2016). The nominal flexural strength of the composite section was 770 kN-m, with the degree of composite action approximately equal to 82% of the yield strength of the steel cross section (W18×35). As shown in Fig. 1(a), a 6×6 W1.4×W1.4 welded wire fabric (3.4 mm diameter plain steel wires in 150 mm grids) was placed in the mid-height of the topping concrete according to the ANSI/Steel Deck Institute (ANSI/SDI) C-2017 (SDI 2017) requirement for shrinkage reinforcement (0.075% of gross concrete area).

Fig. 1(c) illustrates the investigated shear connections using L127×76×9.5 steel angles for double-angle connections and an 11 mm thick steel plate for shear-tab connections, made of A36 (ASTM 2014) steel. The connections were bolted to the beam web using three 19 mm diameter high-strength structural steel bolts spaced at 76 mm and welded to a sacrificial plate attached to the column flanges using 8 mm fillet welds (E70XX electrodes). A 44 mm thick bearing plate was also placed on the outer face of the column flange to minimize damage to the columns. The bottom flanges of the steel beams were coped only for the specimens with double-angle connections. The nominal shear strength of the double-angle connection (360 kN) was governed by weld shear fracture; that of the nominal shear-tab connection (330 kN) was governed by shear fracture of bolts. Four No. 4 reinforcing bars (762 mm in length), distributed along the slab width at 45.7 cm spacing on average, were used for crack control in the concrete slab over the girders.

The ASTM standard coupon tests were conducted to measure the ambient mechanical properties of the steel components. The measured yield and ultimate tensile strengths were 360 MPa and 470 MPa, respectively, for the W18×35 beams; 380 MPa and 510 MPa for the angles; and 350 MPa and 490 MPa for the shear tabs. The measured ultimate strength for bolts, shear studs, and welded wire fabrics was 960 MPa, 510 MPa, and 760 MPa, respectively.

The concrete mixture was designed to provide a lightweight aggregate concrete with a low propensity for thermally-induced spalling. Monofilament polypropylene microfibers of 2.37 kg/m^3 and an expanded slate lightweight aggregate with low water-retention characteristics and high desorption were used as suggested in Pour-Ghaz et al. (2012). The specimens tested under fire loading were cured at an average temperature of 29°C and an average relative humidity of the air equal to 34.5%. The mean 28-day concrete strength was 45.4 MPa. After curing for 6 months, internal relative humidity in the concrete dropped to about 80%. The fire experiments were conducted about 1 year after the concrete placement.

To comply with standard U.S. practice, the steel beams were designed to achieve a 2-hour fire-resistance rating with a commercially-available SFRM product that conforms to the IBC requirements for high-rise buildings with the height between 23 m and 128 m. The manufacturer's specified minimum density of SFRM was 352 kg/m^3. The measured average thickness of applied SFRM was 18 mm for the W18×35 steel beams and 29 mm for the beam-to-column connections. The variation in SFRM thickness was approximately 10 % among the specimens tested in fire. The SFRM thickness of the connections was similar to the thickness required for the 3-hour fire-resistance rating of W12×106 columns.

Test matrix

Table 1 shows the test matrix with the investigated variables including two types of simple shear connections (welded-bolted double-angle versus shear-tab connections) and the presence or absence of slab continuity over the girders. For the specimens with slab continuity (CB-DA-SC and CB-SP-SC), both the welded wire fabric and No. 4 reinforcing bars (used for crack control over support girders) were anchored at the centerline of the columns as shown in Fig. 1(c).

The first specimen (CB-DA-AMB) was tested at ambient temperature to investigate the behavior, failure modes, and ultimate moment capacity (M_{ua}) at midspan, as presented in Choe et al. (2018). The remaining four specimens were tested under compartment fire conditions with the heat release rate of 4000 kW. These specimens were subjected to the gravity load equivalent to the ASCE 7 load combination for extraordinary events (1.2×dead load + 0.5×live load), which required the total mechanical load of 106 kN applied using hydraulic actuators. The resulting flexural load (M) on these specimens at midspan was approximately equal to 45% of M_{ua}.

Structural Setup

Fig. 1(d) shows the test setup. The specimens were attached to the W12×106 columns via simple shear connections in Table 1. The length of the steel beam, the center-to-center distance between the bolt lines on the beam web, and the distance between the centerlines of the two columns were 12.3 m, 12.2 m, and 12.8 m, respectively. As shown in Fig.1(e), a set of brace modules was used to laterally brace the columns at the location of the beam-end connection, which simulated restraints to thermal elongation or contraction of the composite beam specimen. The measured lateral stiffness of the braced column was approximately equal to 180 kN/m on average.

The composite beam specimens were loaded at six points using three loading beam assemblies as shown in Fig. 1(d). The north and south ends of each loading beam were connected to hydraulic actuators (mounted in the basement) via steel tension bars although they are not shown in Fig.1 (e). Forces applied at the ends of the loading beams were transferred to the specimen via loading trusses which were pin-connected at midspan of the loading beams. Steel roller bearings were placed at the interface of the loading trusses and the concrete slab to minimize friction effects. As shown in Fig. 1(f), the sides of the concrete slab of the specimen were laterally braced at three points (spaced 4.3 m apart), using the braces attached to the loading beam. These braces helped to prevent tilting of the concrete slab while the long-span specimen was loaded under fire condition. The loading beams were mechanically guided to move vertically together with the specimen and maintained level using displacement control of the connected actuators. Simultaneously, the total mechanical loads applied on the specimen remained nearly constant using force control of the actuators.

Fire Compartment and Basis of Test Fires

Figs. 1(d) and 1(g) show the front view and inside of the fire compartment constructed below the 12.8 m long specimen. The opening (ventilation) area was approximately 5 m^2. Natural gas was used as the fuel because it allowed independent and near-instantaneous control of heat release rate during the experiment. Three burners (1 m × 1.5 m in plan) with a rating up to 4000 kW each were used to distribute the fire throughout the test compartment. The enclosing walls were constructed of sheet steels on steel studs protected by two layers of 25 mm thick ceramic blankets on the side exposed to a fire.

The fire loading was designed to represent realistic conditions and to have the potential to threaten a structure. The heat release rate used for this study was based upon knowledge gained in previous full-scale fire experiments at the NIST (Hamins et al. 2008) and at the Cardington (BRE 2004). Refer to Table 2 for the detailed comparison of key geometric and thermal parameters used in the previous studies to those used in the current study. The fire was designed to provide an upper layer gas temperature on the order of 1000°C, while minimizing the level of smoke and avoiding excess fuel feeding a fire external to the test compartment. The ventilation was controlled by the total vent area and the height of the vents. When scaled with the compartment volume, the vent area in the current study was slightly greater than that used in the Cardington test in which a fire became ventilation controlled after flashover occurred. Calculations using the NIST Fire Dynamic Simulator (McGrattan et al. 2013) support the hypothesis used in this study that most of the heat content of the natural gas was released within the test compartment with little excess air, simulating an over-ventilated compartment fire.

Surveys (Vassart et al. 2014) have found that the fuel loads in commercial and public spaces vary greatly with the designated purpose of the space. A standard office contains in the range of 420 MJ/m^2 to 655 MJ/m^2 of combustible material; a shopping center is in the range of 600 MJ/m^2 to 936 MJ/m^2; and a library can have fuel loads up to 2340 MJ/m^2. Because the current experiments represented severe fire conditions to attain structural failure, the fuel load considered in this study was in the range of 600 MJ/m^2 to 1200 MJ/m^2 for a two-hour fire. The fires used in the study were not intended to represent a specific scenario; rather, insight was sought into the limit states of conventionally-designed composite beams engulfed in fire for a period beyond their standard 2-hour rating.

Instrumentation

Measurements were performed to characterize the fire loading as well as the thermal and structural responses of the specimens. The heat release rate of the natural gas burners used to control the fire was measured using fuel flow as described in Bryant at al. (2015). The resultant heat release rate in the 13.7 m by 15.2 m exhaust hood was measured using oxygen consumption calorimetry (Bryant et al. 2004).

Fig. 2 illustrates the instrument layout, showing the location of sensors installed in the west half of the specimen. The labels inside the parentheses indicate the same sensors located on the east side of the specimen at the symmetric location. There were total of six locations to measure the vertical displacement of the specimen using position transducers (VD1 through VD4) as well as using the actuators (DispW and DispE). Two dual-axis inclinometers were used to measure the end rotations about the strong axis of the steel beam (RotEx and RotWx) and slope of the concrete slab in the north-south direction (RotEy and RotWy). Temperatures of the specimens were measured at eight locations along the length, sections 1 through 8 as shown in Fig. 2(b). Fig. 2(c) shows the thermocouple layout across the cross section of the specimen at each of eight sections. Glass-sheathed 24-gauge type-K thermocouples were initially used, but for specimens CB-DA, CB-DA-SC, and CB-SP-SC, glass insulation of lead wires exposed to the flames burned off around 10 min after fire ignition, causing secondary junctions in the thermocouple wires. For the last specimen (CB-SP-SC), thermocouple wires were protected by embedding them under a layer of SFRM on the steel beam. For specimens CB-DA-SC, CB-SP, and CB-SP-SC, Inconel-sheathed type-K thermocouples were added to measure the bottom flange temperatures, STC1 through STC4 in Fig. 2(b). Fig. 2(d) shows the thermocouple layout in the connection region.

To measure the average upper layer gas temperature, eight thermocouples, distributed along the beam length, were installed 81 cm below the steel deck of the specimens. Three plate thermometers were used in two specimens, CB-SP and CB-SP-SC, to measure the gas temperature and heat flux i) on the east compartment wall 86 cm below the steel deck, ii) at 6 cm below the bottom flange near mid span, and iii) at 10 cm from the middle web of the steel beam near midspan.

The change in thermally-induced axial loads at the beam ends was measured using strain gauges mounted on the brace modules attached to the columns. For the specimens with slab continuity, CB-DA-SC and CB-SP-SC, tensile forces developed on the no.4 reinforcing bars were measured using load cells.

Details of the measurement uncertainty are presented in Ramesh et al. (2019) and are briefly summarized herein. The expanded uncertainty (with a coverage factor of 2) was estimated to be approximately ± 10 % for applied loads, ± 5 % for displacements, ± 10 % for temperatures without dislodging of thermocouples, ± 2 % for heat release rates measured using burners, and ± 15 % for heat release rates measured using calorimetry.

Testing Procedure and Termination Criteria

The composite beam specimens used in this study were subjected to combined gravity and fire loading as follows:

1. A total mechanical load of 106 kN was applied using hydraulic actuators at ambient temperature and held constant under fire conditions. This load was determined based on the ASCE 7 load combination for fire conditions (1.2×dead load + 0.5×live load).
2. After ignition of a pilot flame on each burner, the heat release rate was initially set to or below 500 kW for about 5 min to verify the uniformity of natural gas flow to all burners. Subsequently, the heat release rate of the burners was linearly increased to 4000 kW over approximately 10 min

and held constant until the mechanical loading was removed when either a preset load or displacement criterion was met (criteria provided below).

3. For specimens not exhibiting failure of beam-to-column connections in Step 2, a cooling phase (decay of the fire) was simulated by linearly decreasing the heat release rate of the burners over 30 min.

Two criteria were used to trigger the removal of the applied mechanical loading in Step 2. For the first specimen tested in fire (CB-DA), a load limit was utilized such that the mechanical loading was automatically removed when the total applied load dropped below 90 kN, 85 % of the total applied load at ambient temperatures in Step 1. For the remaining specimens (CB-DA-SC, CB-SP, and CB-SP-SC), a displacement limit was employed instead. All six actuators were simultaneously depressurized when the vertical displacement of the specimen exceeded 630 mm (equivalent to $L/20$, where L is the nominal length of the specimen). The test was set to be terminated when one of the following criteria was met: 1) incipient collapse of the specimens caused by failure of beam-to-column connections, 2) significant flame leakages above the concrete slab, 3) the loss of exhaust hood flow, 4) significant damage to the fire compartment, 5) failure of data acquisition systems, or 6) the end of the 30-min decay period.

Results and Discussion

Imposed Gravity and Fire Loading

Fig. 3 shows the total gravity load (P) applied using actuators and the heat release rates of natural gas burners (HRR_B) as a function of time measured after ignition of a fire. For all specimens, the time-averaged value of P was 106 kN with the variation below 3%. Specimens CB-DA-SC and CB-SP exhibited fluctuations in applied loads over time, related to misadjustment of the electrohydraulic servo valve used in one of the six actuators. This servo valve was replaced before testing the last specimen (CB-SP-SC), and the load variations (over time) fell to approximately 1%.

While the specimens were loaded mechanically, thermal loading was applied using the natural gas burners inside the compartment. Similar fire conditions were achieved in all four tests. The value of HRR_B ramped to 4000 kW at an average rate of 400 kW/min and then maintained constant (1% variation over time). Specimen CB-DA was unloaded at 30 min, triggered by a 15 % reduction in total mechanically-applied gravity loads (a preset load limit) due to local buckling of the beam ends. The displacement limit of $L/20$ resulted in unloading of CB-DA-SC at 63 min. For these specimens, the 30-min cooling phase began since no incipient collapse was exhibited. For the other two specimens (CB-SP and CB-SP-SC), both the mechanical and thermal loading was manually removed at 65 min and 73 min, respectively, followed by failure of the east shear-tab connection.

Heat Release Rate and Gas Temperature

Fig. 4 shows the heat release rate measured at the exhaust hood and the average gas temperatures 81 cm below the steel deck of the specimens as a function of time after fire ignition. The increase of heat release rates was about 10% slower than HRR_B in Fig. 3. Around 20 min after ignition, the heat release rates remained steady. For CB-DA-SC, the time-averaged value of heat release rate was about 3700 kW; for other three tests it was 3900 kW on average. The standard deviation over time was 3% until the cooling phase was initiated.

The compartment fires produced using natural gas burners created hot flammable gases trapped below the specimens. As shown in Fig. 4, the evolution of gas temperatures followed the heat release rates varying with time and exhibited a similar trend for all specimens except the cooling phase as follows. The average gas temperature reached 900°C around 15 min after ignition and continuously increased while the heat release rate was maintained around 4000 kW. The maximum temperature was 1020°C at 40 min (CB-DA) and 1070°C at 73 min (CB-SP-SC). The temperature variation along the beam length was less than 50°C, implying that approximately uniform gas temperatures were achieved at exposed surfaces of the specimens.

Figs. 4(c) and 4(d) show temperatures measured using a plate thermometer (PT) mounted at the bottom flange near midspan, comparable with the average gas temperature measured using thermocouples. For CB-SP and CB-SP-SC, the time-averaged value of heat flux calculated using the bottom flange PT data ranged from 130 kW/m^2 to 200 kW/m^2 estimated between 20 min and 65 min after fire ignition.

Temperature Response

Fig. 5 shows surface temperatures measured at various locations of the specimens, including exposed steel deck, the bottom flange of W18×35 steel beams, shear connections (angles or shear tabs), and the top and bottom surfaces of the middle portion of the concrete slab (in contact with the top flange of the steel beam). The temperatures shown are the average temperature measured using thermocouples relevant to each location (Fig. 2). The bottom flange temperatures were measured using the Inconel-sheathed thermocouples due to insulation failure of glass-sheathed thermocouples.

As shown in Fig. 5, temperatures of the steel deck reached 600°C before 15 min and increased to 1000°C or higher before cooling. The deck thermocouples attached to CB-DA fell off about 10 min after ignition. The variation in temperatures of the steel deck along the beam length was as large as 20% during the first 15 min but decreased with time, falling below 2%. Similarly, temperature rises of the SFRM-protected bottom flange of W18×35 steel beams were comparable among CB-DA-SC, CB-SP, and CB-SP-SC until 60 min; the average temperature exceeded 600°C at 45 min after ignition and reached nearly 800°C at 70 min. The average heating rate of the protected bottom flange was 10°C/min estimated between 30 min and 65 min. The difference in temperatures measured between two Inconel-sheathed thermocouples at 2.5 m apart (Fig. 2) ranged from 20°C to 100°C until the cooling phase began. This discrepancy could be caused by cracks in the SFRM due to deformation of the steel beam during fire loading.

As shown in Fig. 5, the average temperatures of beam-to-column connections protected with a thick layer of SFRM was much lower than those of the protected steel beams. The connection temperatures continued to increase through the early phase of cooling up to 40 min but never exceeded 300°C. The variation in temperatures measured at discrete locations in the connections (Fig. 2) was below 30°C. The maximum temperature at the bottom surface of the concrete slab (in contact with the top flange of the steel beam) was in the range of 200°C to 300°C, achieved during cool-down. The temperature of the unexposed (top) surface of the concrete never reached over 100°C.

Fig. 6 shows a typical temperature distribution across the section of CB-SP-SC. The plotted values are the average temperatures measured at each location in the sections 3 through 6 in Fig. 2. The lower portion of the protected W18×35 beam (i.e., T13 through T15) rapidly reached the temperature ranging from 650°C to 700°C at 60 min. A peak temperature at each thermocouple location of the W18×35 section ranged from 500°C to 740°C when the fire was extinguished at 73 min. On the other hand, thermal gradients were developed within a concrete slab. As shown in Fig. 6(b), the maximum temperature measured at the middle portion of the concrete slab (T6, T8, and T10) was below 300°C. The bottom surface temperature of the concrete slab measured 46 cm from the beam centerline (T5) increased to a temperature ranging from 840°C to 910°C at 73 min before extinguishment of the fire. Temperatures of the top (unexposed) surface (T1 and T6) remained below 100°C during heating, but the temperature at T1 increased to nearly 140°C during cooling.

Measured temperature of specimen CB-SP-SC indicated that the web and the bottom flange of the protected steel beam was uniformly heated along the beam span with the variation less than 10% during heating. A larger temperature variation (20%) was achieved at the top flange of the steel beam because of the heat sink provided by the concrete slab and thicker SFRM coating applied at the interface with the steel deck. Although temperature of the concrete was generally much lower than that of other steel components, rapid variation in temperatures reached as large as 80% because of concrete cracks and evaporation of moisture.

Vertical Displacement and End Rotation

Fig. 7(a) shows the average vertical displacements of the specimens measured at 91.4 cm from midspan (VD2 and VD3 shown in Fig.2) as a function of the test time recorded after the fire ignition. The negative values indicate a downward displacement. Among the tested specimens, a similar trend was observed during fire exposure. Following the fire ignition, the specimens continuously bent downward until cooling was initiated. The displacement rate started rapidly increasing after 15 min to 20 min from ignition. Local buckling at the beam ends occurred when the vertical displacement was approximately equal to 115 mm (*L*/110). For the specimens with slab continuity (CB-DA-SC and CB-SP-SC), the concrete slab in the negative moment region appeared to be fractured between 50 min and 60 min from ignition, and smoke and flames were visible on the top (unexposed) surface of concrete. The vertical displacement corresponding to this event was about *L*/40.

It is important to note that two different criteria were used for unloading of the specimens, including a load limit (15% reduction in applied loads) for the CB-DA specimen and a displacement limit (L/20) for the remaining specimens. The maximum vertical displacements of the tested specimens (Fig. 7(a)) and associated events observed in this study are summarized as follows.

1. CB-DA: Unloading occurred at 30 min due to exceedance of the preset load limit for the actuators, triggered by local buckling of the beam ends. The unloaded specimen continuously sagged throughout a 30-min decay period of the fire. The peak vertical displacement was 330 mm (approximately *L*/40) before the fire was extinguished.
2. CB-DA-SC: The vertical displacement increased continuously even after unloading was triggered at 63 min (due to the *L*/20 limit of actuators). The maximum value was approximately equal to 690 mm (*L*/18) at 90 min. The fire was extinguished at 94 min. This specimen collapsed by weld fracture of the east double-angle connection during cooling, about 5 hours after the fire extinguishment. The vertical displacement at collapse was not recorded.

3. CB-SP: When the vertical displacement reached 550 mm (L/23) around 65 min after ignition, the specimen collapsed by weld failure of the east shear-tab connection. This specimen was arrested at a vertical displacement of 690 mm by catch beams shown in Fig. 1. Mechanical loads and fire loading were removed immediately. The displacement change at 130 min was caused by further damage in the east connection region (concrete, connection elements, or both) during cooling.
4. CB-SP-SC: The vertical displacement was 580 mm (L/22) when the bottom bolt used in the east shear-tab connection failed around 73 min after ignition. Mechanical loads and fire loading were removed immediately. However, the specimen further bent downward, reaching a peak displacement value of 590 mm at 10 min of cooling. About 3 hours into cooling, the vertical displacement recovered to 370 mm, followed by collapse of the specimen due to fracture of the remaining bolts in the east shear-tab connection.

Fig. 7(b) shows the average end rotations of the CB-DA and CB-SP specimens as a function of the test time recorded following ignition of the test fire. The positive values indicate the end rotations caused by sagging of the specimens. During first 10 min of heating, end rotations barely increased due to the limited rotational restraint provided by the beam-end connections. However, the double-angle connection exhibited more ductile behavior afterwards. Although the CB-DA specimen was unloaded at 30 min, the end rotation increased linearly at a rate of 2×10^{-3} rad/min until 50 min. A peak value of 0.09 radian was achieved at 63 min (during decay of the fire). The end rotations of CB-SP increased much slowly from 20 min to 50 min (at a rate of 9×10^{-4} rad/min) and substantially increased at a rate of 5×10^{-3} rad/min until 63 min. A runaway rotation was achieved at 65 min followed by failure of the east shear-tab connection.

Flexurual Capacity and Effects of Thermal Restraint

Fig. 8(a) shows the temperature-dependent flexurual capacity of the composite beam specimens, plotted with the test time recorded after the fire ignition. Since strain measurement was not made in this study, the measured bottom flange temperature and the retention factors specified in Table A-4.2.4 of the AISC 360 specification were used to estimate the flexural (plastic) capacity of the composite section. As shown, the flexural capacity of the specimens started decreasing substantially after 30 min (400°C). The CB-DA-SC and CB-SP-SC specimens appeared to be reached full plastic yielding at 60 min (710°C) at midspan as the flexural capacity became equal to the applied moment (M). According to the AISC approach, the CB-SP specimen collapsed (by connection failure) before flexural yielding occurred.

The composite beam specimens were restrained by the laterally-braced W12×106 columns connected via simple shear connections (Fig. 1(e)). As shown, the ends of the specimens including connections were subjected to compression exerted from the restraint to thermal elongation. The compressive load increased until local buckling occurred at the beam ends and then started decreasing, eventually turning into tension either at very large vertical displacements during heating, so-called 'catenary action', or due to the restraint to thermal contraction during cooling.

Fig. 8 (b) shows the average axial loads measured at the ends of the specimens as a function of the bottom flange temperature. The negative values represent compression. Some observations made in this study are as follows:

1. Local buckling occurred at the bottom flange temperature in the range of 400℃ to 500℃, prior to yielding of the composite section (at 710℃).
2. The local buckling capacity (P_u) of the CB-DA and CB-DA-SC specimens was 725 kN on average and that of the CB-SP and CB-SP-SC specimens was 990 kN on average. This difference was thought to be resulted from the coped bottom flanges used in the CB-DA and CB-DA-SC specimens (i.e., the reduced cross-sectional area of the steel beam subjected to compression).
3. The presence of the end slab continuity led to a higher buckling capacity when the shear-tab connection was used. The P_u of CB-SP-SC was approximately 7% higher than that of CB-SP. The difference in P_u between CB-DA and CB-DA-SC was around 1%.

4. The tensile capacity (T_u) of the shear tab connection was 85 kN for CB-SP and 105 kN for CB-SP-SC, approximately equal to 25 % of the ambient shear capacity calculated using the AISC 360 and measured mechanical properties.
5. The double-angle connection appeared to have a higher tensile capacity (or ductility capacity) than the shear-tab connection. As shown in Fig. 8(b), the shear-tab connection failed at 105 kN around the bottom flange temperature of 145°C (CB-SP-SC) whereas the induced tensile load on the double-angle connection was 120 kN at similar temperature (CB-DA-SC). This double angle connection failed around 5 hours of cooling.

For the CB-DA-SC and CB-SP-SC specimens, the slab continuity over girders was achieved by anchoring the slab reinforcement (both the No.4 reinforcing bars and welded wire fabric used for crack control) at the centerlines of support columns. Fig. 8(c) shows the total tensile loads on the east and west No.4 bars versus the time recorded after the fire ignition. An initial load variation at the time of ignition was resulted from posttensioning of the bars during the installation of load cells and gravity loading applied at ambient temperature using actuators. Between 22 min and 26 min after ignition, the tensile load on the bars decreased to nearly zero since the concrete slab was subjected to compression due to the restraint against thermal elongation. When the beam ends buckled (at 30 min for CB-DA-SC and at 40 min for CB-SP-SC), the tensile load on the bars sharply increased. This was thought to be because of a plastic hinge formed at the location of local buckling, and thereby there was an increased demand in the anchored bars to carry the negative moment. Fluctuation in loads was followed due to concrete cracking and associated bond slip of the bars as the moment increased. The tensile load corresponding to the negative moment capacity of the concrete slab was in the range of 100 kN to 110 kN (equivalent to 30% of the ambient tensile strength of the reinforcing bars), which occurred around 50 min for CB-DA-SC and 65 min for CB-SP-SC. At this load level, the welded wire fabric in the negative moment region was fractured and bond slip failure of No.4 bars occurred. Smoke and flames from the fractured concrete became visible. Therefore, a tensile membrane action of the concrete slab was not observed in this study.

Failure Modes

The specimens used in this study reached various limit states during the heating and cooling phases. Fig. 9 shows selected photographs of the specimens after cooling. Additional data and photographs are presented in Choe et al. (2019). The observed modes of structural failure are discussed as follows.

Local Buckling

All specimens exposed to fires exhibited local buckling of the W18×35 steel beams near the beam-to-column connections, as shown in Fig. 9(a). It appeared that the geometry of the beam end section influenced the location of local buckling. The CB-DA and CB-DA-SC specimens had a T-shaped end section owing to the coped bottom flange. Both specimens exhibited web local buckling approximately 20 cm from the beam end, resulting in fracture of the bottom web toe of fillet at the east coped bottom flange. This fracture might cause a sudden reduction in applied loads for CB-DA which was unloaded after local buckling occurred. On the other hand, the CB-SP and CB-SP-SC specimens exhibited local buckling both at the bottom flange and at the web, about 60 cm from the beam ends.

Flexural Failure

For all specimens exposed to fire, the steel beams exhibited permanent deflections associated with flexural failure (Refer to Fig. 9(b)); however, there was no significant damage to the SFRM coating on the deformed steel beams at midspan. Neither spalling nor crushing of the concrete slab was observed. For the specimens with slab continuity (CB-DA-SC and CB-SP-SC), the concrete slab fractured near the east and west ends due to negative flexure although dissimilar crack patterns were observed. As shown in Fig. 9(c), the CB-DA-SC specimen exhibited V-shaped cracks on the top of concrete. The valley of this crack was located about 20 cm from the end of the steel beam, similar to the location where web local buckling occurred. However, the CB-SP-SC specimen showed flat fractures in concrete along the slab width above the location of flange local buckling, approximately 66 cm from the end of the steel beam.

For both specimens, the welded wire fabric ruptured at the crack planes, but the No.4 reinforcing bars did not yield.

Unlike the ambient specimen (CB-DA-AMB) which failed by shear rupture of the first headed stud at the east end (Choe et al. 2018), the CB-DA and CB-SP specimens indicated negligible shear deformations of the end studs. However, according to the post-test inspection, the CB-DA-SC and CB-SP-SC specimens had the end studs that exhibited tensile fracture of the shank above weld joints and concrete breakout failures. Although the exact cause of this failure needs to be further investigated, it is speculated that the end studs could be subjected to a large uplift force due to the negative moment caused by the rotational restraint of the slab continuity.

Connection Failure

The simple shear connections used in this study exhibited various failure modes, as shown in Fig. 9(d). The welded-bolted double-angle connections indicated failure in weld joints of the angle legs on the column face. For CB-DA, partial weld fractures were witnessed after cooling, whereas full fractures of welds, so-called ‘unzipping’, happened during cooling of CB-DA-SC. The angle legs welded on the column face were also permanently bent (yielding). The slab continuity appeared to influence the failure characteristics of shear-tab connections used in this study. The east connection of CB-SP failed by weld facture during heating. For CB-SP-SC, the bottom bolt connected to the east shear tab fractured during heating and the remaining bolts in the same connection fractured during cooling. Provided that a similar fire exposure (with the heat release rate of 4000 kW) and mechanical loading were used in this study, the angle connection (failed about 5 hours after the fire extinguishment) appeared to be more robust compared with the shear tab connection (failed about 3 hours after the fire extinguishment). When used for connecting long-span beams, however, both connections could present vulnerabilities caused by fire effects.

Summary and Conclusions

This paper presented the results of compartment fire experiments in which the fire performance and failure modes of four 12.8 m long partially-composite beam assemblies resisting gravity loads were evaluated. The variables tested include (1) two types of simple shear connections (welded-bolted double-angle versus shear-tab connections) and (2) the presence or absence of slab continuity over the girders. The applied gravity load was equivalent to the ASCE 7 load combination for extraordinary events (1.2×dead load + 0.5×live load). The 4000 kW compartment fires were produced using natural gas burners to simulate realistic fire loading. The characteristics of imposed mechanical and fire loading as well as thermal and structural responses of the specimens were measured using various instrumentations. The data presented in this paper can guide to develop or validate predictive tools used for performance-based design of structures in fire.

Test results indicated that the compartment fires produced repeatable, uniform heating conditions at exposed surfaces of the specimens. The upper layer gas temperatures inside the fire compartment reached over 1000°C before cooling was initiated. The thermal gradient was developed across the section of the specimens. Temperatures of SFRM-coated bottom flanges exceeded 600°C at 45 min after ignition while the top surface of the concrete slab remained below 100°C during heating but increased to nearly 140°C during cooling. The average temperature of the beam end connections increased even after extinguishment of a fire but never exceed 300°C because a thicker SFRM layer was applied.

The specimens exhibited diverse structural responses to fire depending on the end support conditions and achieved various limit states throughout the heating and cooling phases of the fire loading. Some important observations are highlighted below. These observations would not be possible through standard fire testing.

1. There was a significant influence of thermal elongation and contraction on the behavior of the specimens. The axial loading induced by the effect of thermal restraints was enough to buckle the beam ends locally, prior to yielding of the composite section during heating, and to fail the

connections during cool-down. The magnitude and shape of local buckling were affected by the geometry of the end sections of the specimens associated with the connection type; in particular, whether or not the bottom flange of the steel beams was coped.

2. The long-span composite beam specimens supported by simple shear connections maintained their load-carrying capacity in fire at large vertical displacements (nearly $L/20$), through a catenary action. However, the minimum code-required shrinkage reinforcement (0.075% of gross concrete area) was not sufficient to resist thermally-induced negative moments over the girders. Concrete failure in this region could lead to fire spread between floors.
3. The rotation capacity (ductility) of the welded-bolted double-angle connection was greater than that of the shear-tab connections in fire. However, the welded-bolted double-angle connections supporting long-span beams could fail due to large axial restraints against thermal contraction during cooling. The rotational restraint of concrete slabs over the girders affected the behavior and limit states of the shear-tab connections in fire. There could be vulnerabilities in shear-tab connections used in long-span floor construction during both the heating and cooling periods of severe fires, although further study is needed.

Acknowledgements

This work was conducted as part of the project “Measurement of Structural Performance in Fire” under the NIST Engineering Laboratory’s Fire Risk Reduction in Building Programs. We thank William Baker (Skidmore, Owings & Merrill), Craig Beyler (Jensen Hughes), Luke Bisby (University of Edinburgh), Ian Burgess (University of Sheffield), Charles Carter (AISC), Charles Clifton (University of Auckland), Michael Engelhardt (University of Texas), Graeme Flint (Arup), Nestor Iwankiw (Jensen Hughes), Kevin LaMalva (Simpson Gumpertz & Heger), Roberto Leon (Virginia Tech.), and Amit Varma (Purdue University) for their expert consultation. We also thank the NIST colleagues including Brian Story, Laurean DeLauter, Anthony Chakalis, Philip Deardorff, Marco Fernandez, Artur Chernovsky and Ana

Sauca, Joseph Main, and Fahim Sadek for their significant contributions to design, construction and execution of this test program.

References

AISC (American Institute of Steel Construction). (2016). “Specification for Structural Steel Buildings”, ANSI/AISC 360-16, AISC, Chicago, IL.

Alfawakhri, F., Carter, C., Berhing, R., Zeeveld, P., Hervey, F., and Woods, L. (2016). “The effects of load intensity and restraint on the fire resistance of steel and composite beams.” *Proc., 9th Int. Conf. Structures in Fire (SiF)*, Princeton, NJ.

ASCE (American Society of Civil Engineers). (2018). “Structural fire engineering.” *ASCE MOP 138*, Reston, VA.

ASCE (American Society of Civil Engineers). (2016). “Minimum design loads for buildings and other structures.” *ASCE 7-16*, Reston, VA.

ASTM (American Society of Testing and Materials). (2018). “Standard test methods for fire tests of building construction and materials.” *ASTM E119*, West Conshohocken, PA.

ASTM (American Society of Testing and Materials). (2018). “Standard specification for carbon structural steels.” *ASTM A36/A36M*, West Conshohocken, PA.

Bryant, R., Bundy, M., and Zong, R. (2015). “Evaluating measurements of carbon dioxide emissions using a precision source—A natural gas burner.” *J. the Air & Waste Manage. Assoc.*, 65(7), 863-870.

Bryant, R., Ohlemiller, T. J., Johnson, E. L et al (2004). “The NIST 3-megawatt quantitative heat release rate facility.” *NIST SP 1007*, Gaithersburg, MD.

Building Research Establishment (BRE). (2004). “Results and observations from full-scale fire test at BRE Cardington.” *Client Report 215-741*, U.K.

Bundy, M., Hamins, A., Gross, J., Grosshandler, W., and Choe, L. (2016). “Structural fire experimental capabilities at the NIST National Fire Research Laboratory.” *Fire Tech.*, 52(4), 959-966.

Choe, L., Ramesh, S., Hoehler, M., Gross, J. (2018). “Experimental study on long-span composite floor beams subject to fire: baseline data at ambient temperature.” *Proc., Structures Congress 2018*, Fort Worth, TX.

Choe, L. (2019). “Compartment Fire Experiments on Long-Span Composite Beams with Simple Shear Connections. Part 2: Test Results.” *NIST Technical Note 2055*, Gaithersburg, MD. (in press)

Hamins, A. P., Maranghides, A., McGrattan, K. B., Ohlemiller, T.J., and Anleitner, R. (2008). “Experiments and modeling of multiple workstations burning in a compartment.” *NIST NCSTAR 1-5E*, Gaithersburg, MD.

ICC (International Code Council). (2018). *International Building Code,* Country Club Hills, IL.

Kirby, B. (1998). “The behavior of a multi-storey steel framed building subjected to fire attack.” *Experimental data*, British Steel Corporation (now Corus), Rotherham, U.K.

Kordosky, A. (2017). “Experimental and computational investigation of composite beam response to fire.” *Master of Science Dissertation*, Dept. of Civil and Environmental Engineering, Lehigh Univ., PA.

McGrattan, K., Hostikka, S., McDermott, R., Floyd, J., Weinschenk, C., and Overholt, K. (2013). “Fire Dynamics Simulator, Technical Reference Guide, Sixth Edition.” *NIST SP-1018*, Gaithersburg, MD.

Newman, G. M., and Lawson, R. M. (1991). “Fire resistance of composite beams.” *SCI Publication 109*, Ascot, U.K.

NFPA (National Fire Protection Association). (2018). “Building Construction and Safety Code.” *NFPA 5000*, Quincy, MA.

NIST (National Institute of Standards and Technology). (2008). “Final report on the collapse of World Trade Center Building 7.” *NIST NCSTAR 1A*, Gaithersburg, MD.

Pour-Ghaz, M., Castro, J., Kladivko, E., J., and Weiss, J. (2011). “Characterizing lightweight aggregate desorption at high relative humidities using a pressure plate apparatus.” *J Mater Civil Eng*, 24(8), 10.1061/(ASCE)MT.1943-5533.0000422.

SCI (Steel Construction Institute). (2008). *Best practice in steel construction, commercial buildings, guidance for architects, designers, and constructors,* Ascot, U.K.

SDI (Steel Deck Institute). (2017). “C-2017 Standard for composite steel floor deck–slabs.” *ANSI/SDI C-17*, < http://www.sdi.org/wp-content/uploads/2017/02/ANSI-SDI-C-2017-Standard.pdf> (Apr. 12. 2019).

Ramesh, S., Choe, L., Seif, M., Hoehler, M., Grosshandler, W., Sauca, A.,…Glisic., B. (2019). “Compartment Fire Experiments on Long-Span Composite Beams with Simple Shear Connections. Part 1: Experimental Design and Beam Behavior at Ambient Temperature.” *NIST Technical Note 2054*, Gaithersburg, MD. (in press)

Selden, K. L., Fischer, E. C., and Varma, A. H. (2016). “Experimental Investigation of Composite Beams with Shear Connections Subjected to Fire Loading.” *J. Struct. Eng.*, 10.1061/(ASCE)ST.1943-541X.0001381, 04015118.

Vassart, O., Zhao, B., Cajot, L.G., Robert, F., Meyer, U., Frangi, A. (2014). “Eurocodes: Background & Applications Structural Fire Design.” *Report EUR 26698 EN.* European Commission, Luxembourg.

Wainman, D. E. and Kirby, B. R. (1987). “Compendium of UK standard fire test data, unprotected structural steel–1.” *Ref. No. RS/RSC/S10328/1/98/B*, British Steel Corporation (now Corus), Rotherham, U.K.

Zhao, B., and Kruppa, J. (1997). “Fire resistance of composite slabs with profiled steel sheet and of composite steel concrete beams. Part 2: Composite beams.” *Final Rep.*, European Commission, Luxembourg, France.

Table 1. Test Matrix

Test	Specimen name	Connection type	Slab end continuity	M/M_{ua}	Fire load
1	CB-DA-AMB	double angles	not included	1	-
2	CB-DA	double angles	not included	0.45	4000 kW
3	CB-DA-SC	double angles	included	0.45	4000 kW
4	CB-SP	shear tab	not included	0.45	4000 kW
5	CB-SP-SC	shear tab	included	0.45	4000 kW

Note: M = ultimate moment capacity measured at ambient temperature; M_{ua} = applied moment during the fire experiment.

Table 2. Key geometric and thermal parameters used for fire experiments

Parameter	NIST (Hamins et al. 2008)	Cardington (BRE 2004)	Proposed test fire
depth × width × height	10.7 m × 7 m × 3.4 m	11.0 m × 7.0 m × 3.1 m	2 m × 12.8 m × 3.7 m
opening area	4.8 m^2	11.4 m^2	5.9 m^2
fuel package	3 work stations; 40 L of jet fuel	wood cribs	3 natural gas burners (1 m × 1.5 m each)
fuel load	400 MJ/m^2	720 MJ/m^2	600−1200 MJ/m^2
peak HRR/volume	40 kW/m^3	unknown	42 kW/m^3
Peak gas temperature	1050 °C	1050 °C	1000 °C
fire duration	67 min	200 min	60 min to 90 min (with cooling period)

Note: HRR = heat release rate.

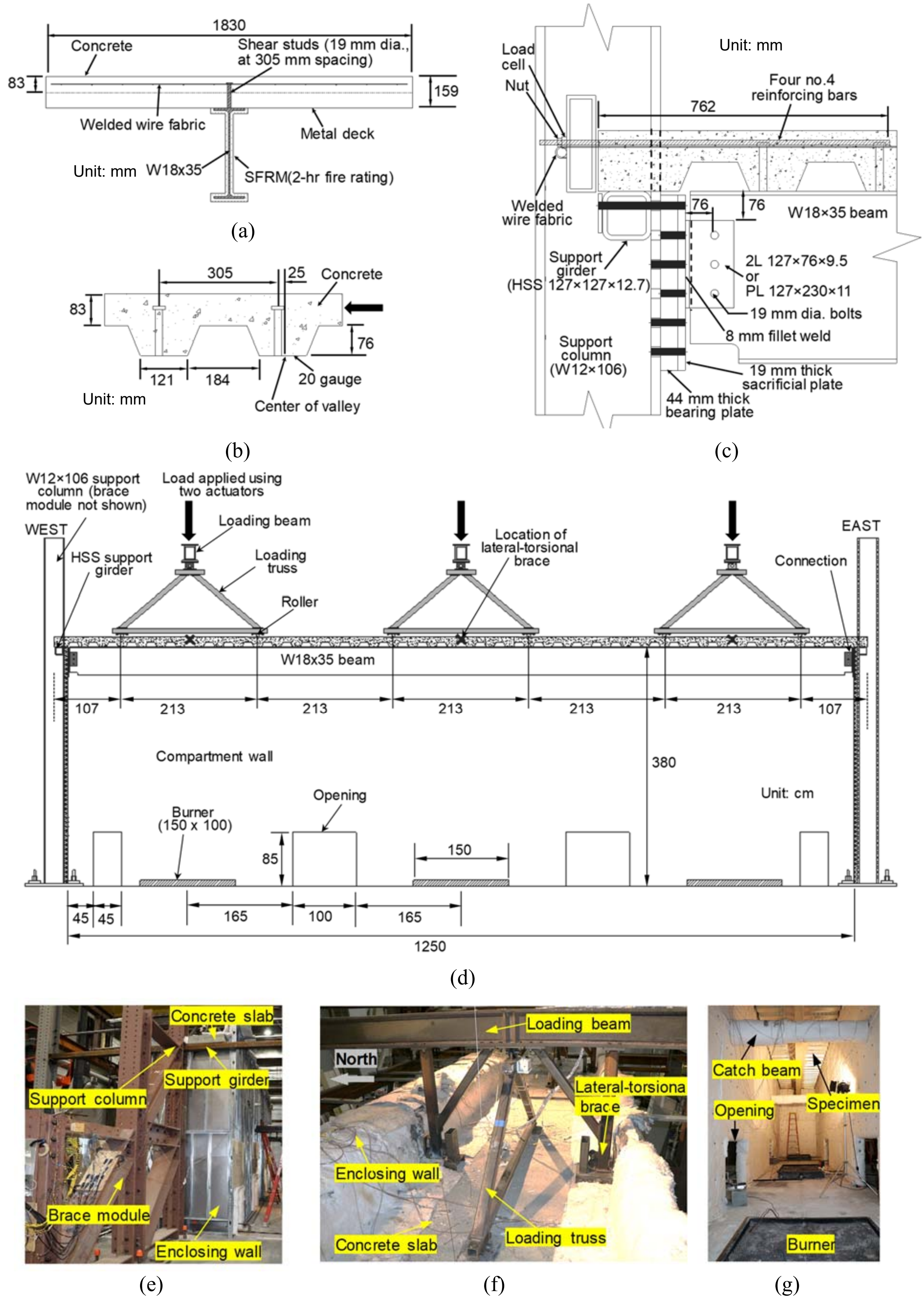

Fig. 1. Scale drawings of (a) specimen cross section; (b) steel deck; (c) end support details; (d) front view of test setup; photographs of (e) support column, (f) loading system, and (g) inside of fire compartment

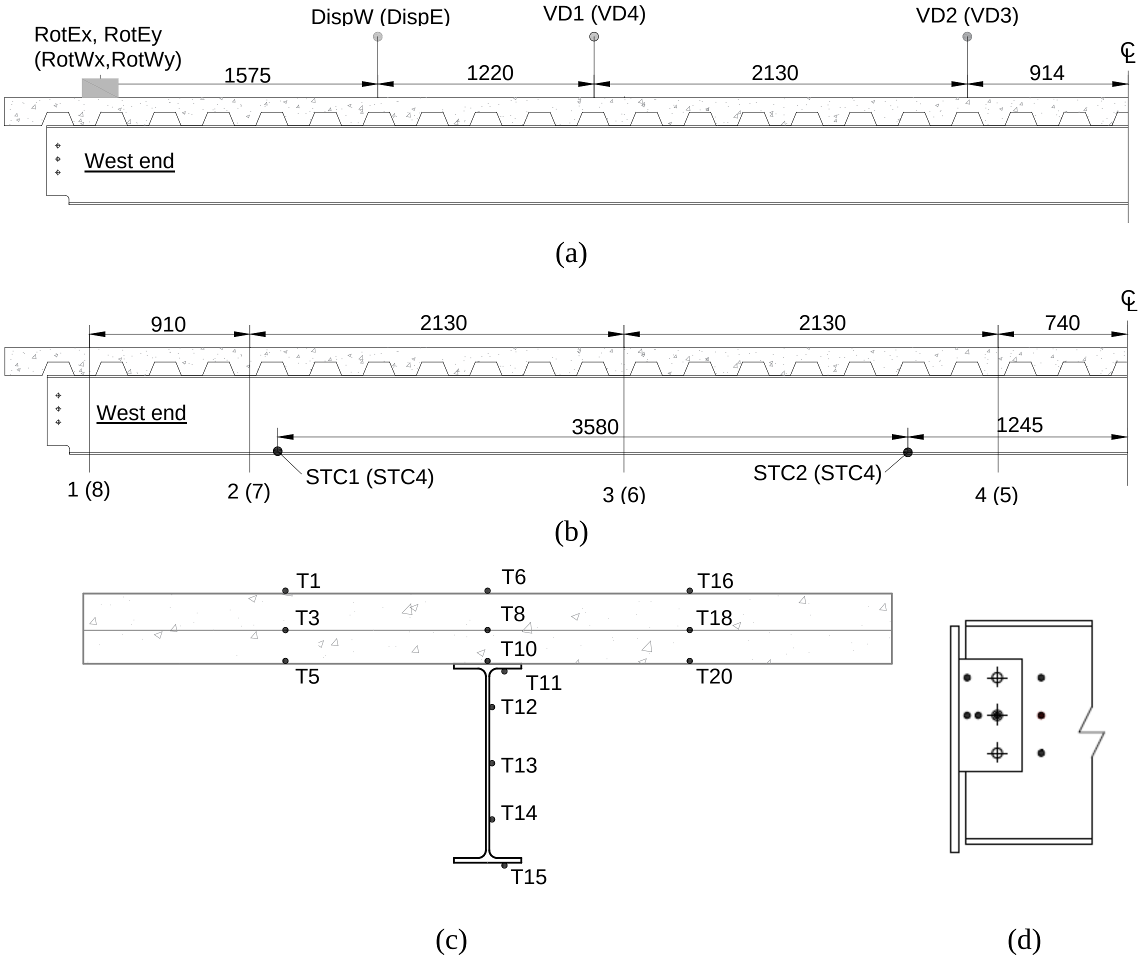

Fig. 2. Scale drawings of instrumentation layout (unit: mm): (a) displacement and rotation; (b) temperature along beam length; (c) temperature in sections 1 through 8; and (d) temperature at connection

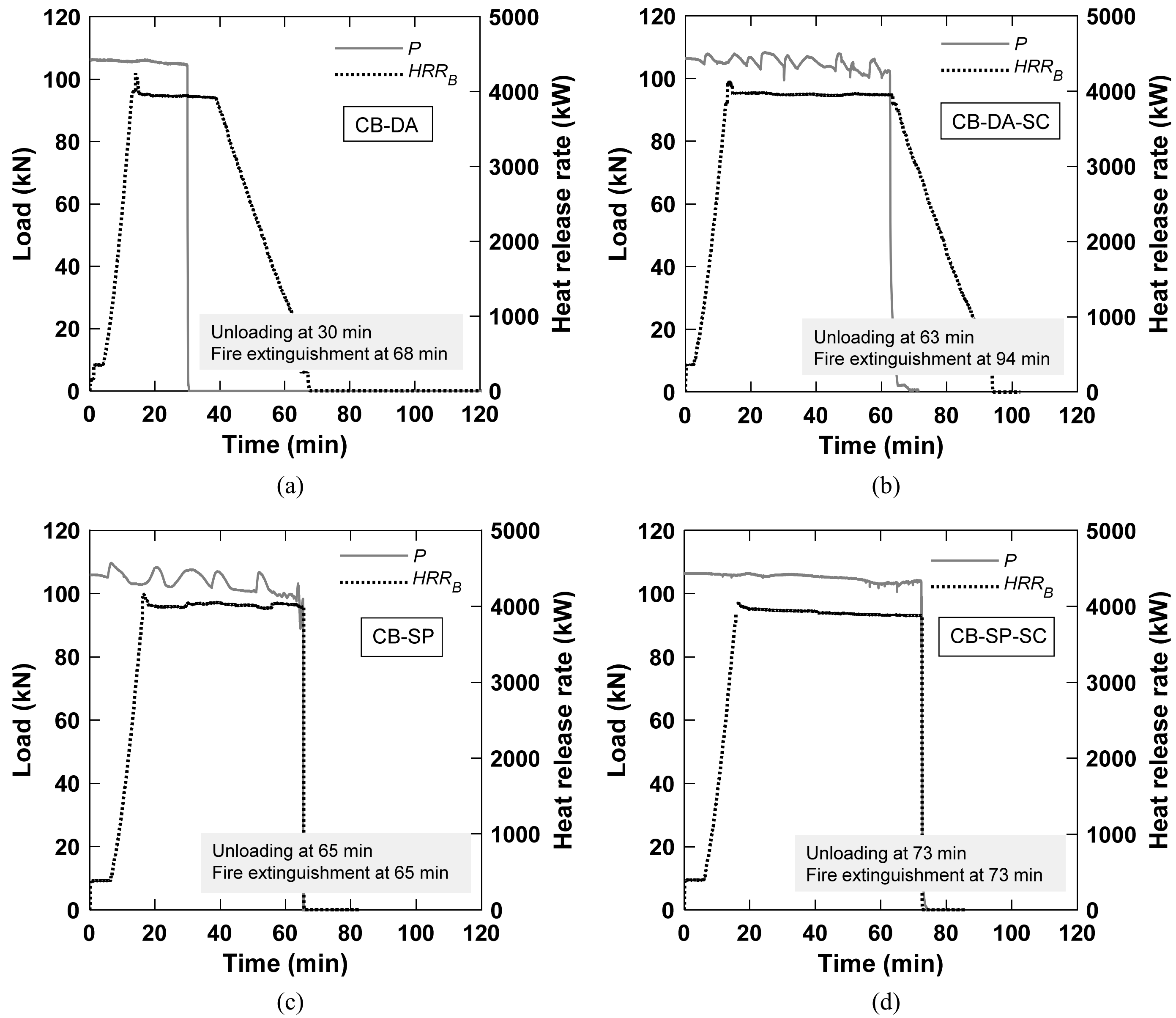

Fig. 3. Total mechanical load (P) and heat release rate of burners (HRR_B) measured for (a) CB-DA; (b) CB-DA-SC; (c) CB-SP; and (d) CB-SP-SC

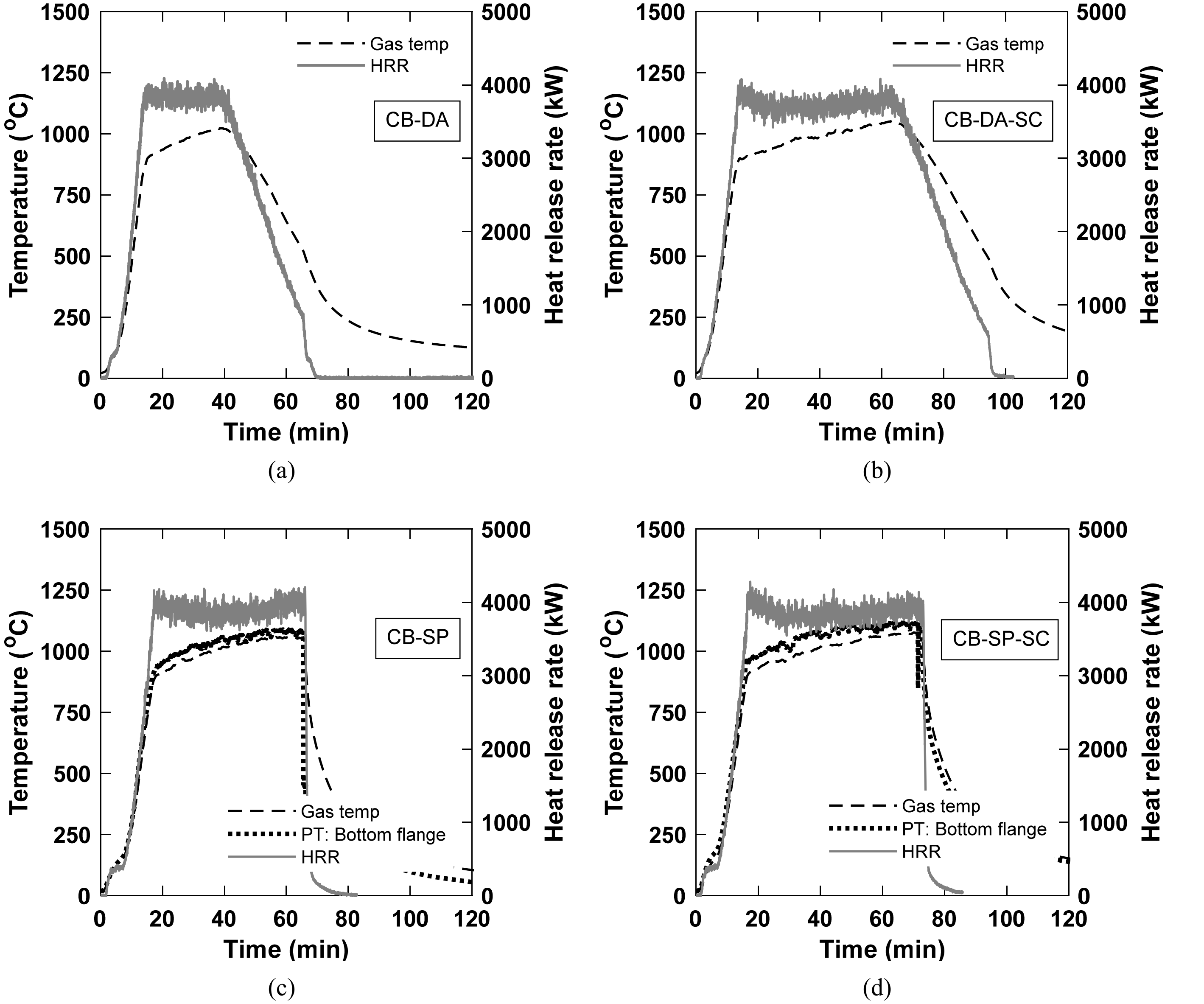

Fig. 4. Heat release rate (HRR) measured at exhaust hood and average gas temperature for (a) CB-DA; (b) CB-DA-SC; (c) CB-SP; and (d) CB-SP-SC; Note: PT1: Bottom flange = gas temperature measured using a plate thermometer mounted at 10 cm below bottom flange at midspan for CB-SP and CB-SP-SC

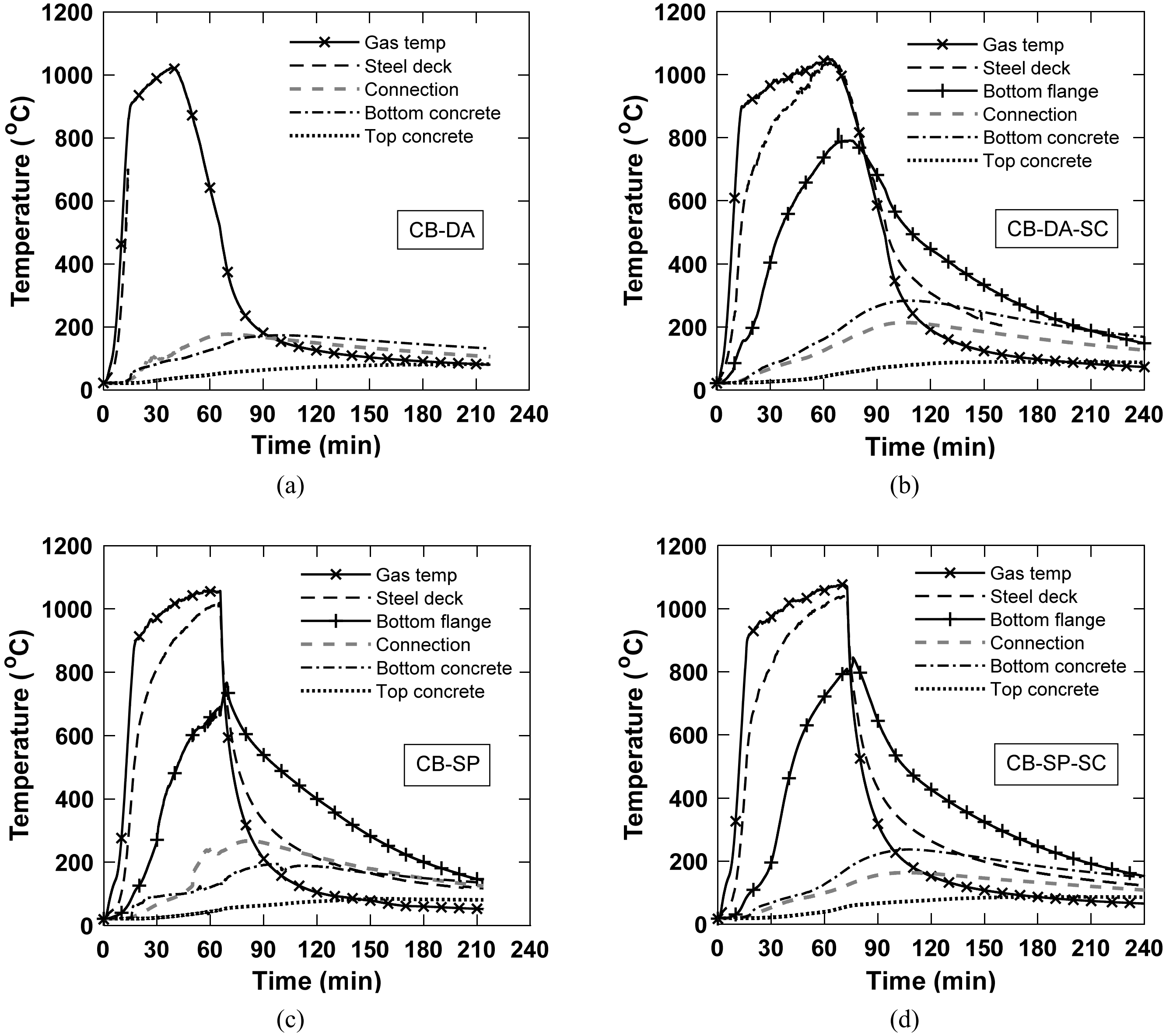

Fig. 5. Surface temperatures measured at various locations of (a) CB-DA; (b) CB-DA-SC; (c) CB-SP; and (d) CB-SP-SC along with average gas temperature

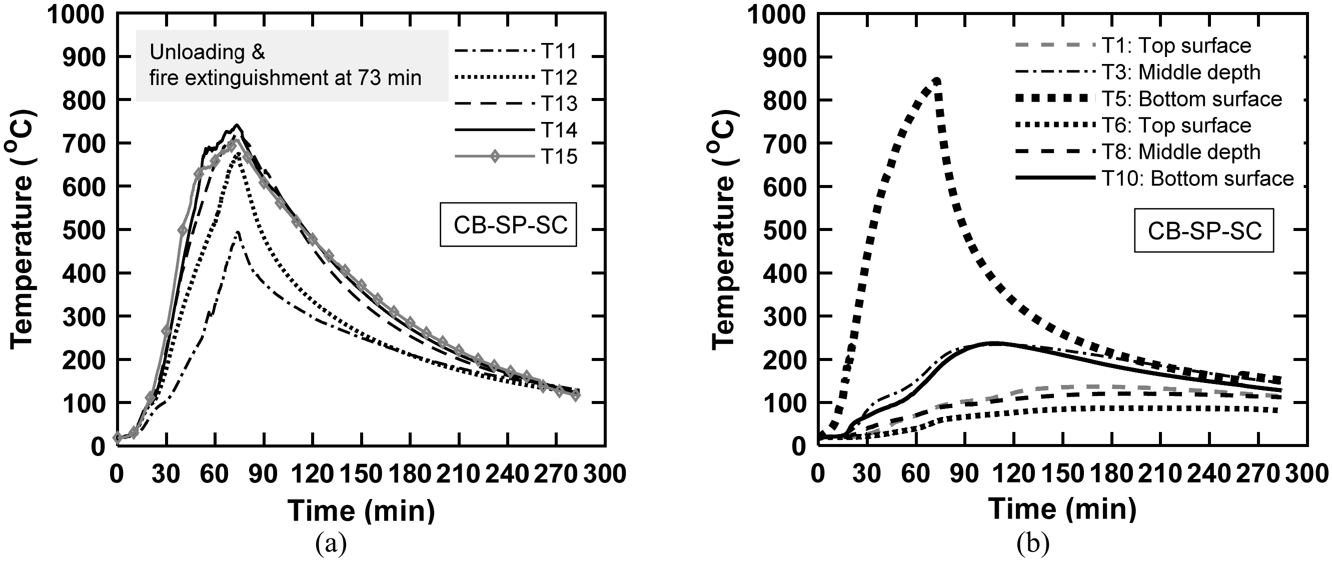

Fig. 6. Temperature of (a) W18×35 steel beam and (b) concrete slab of CB-SP-SC, measured using thermocouples shown in Fig. 2(c)

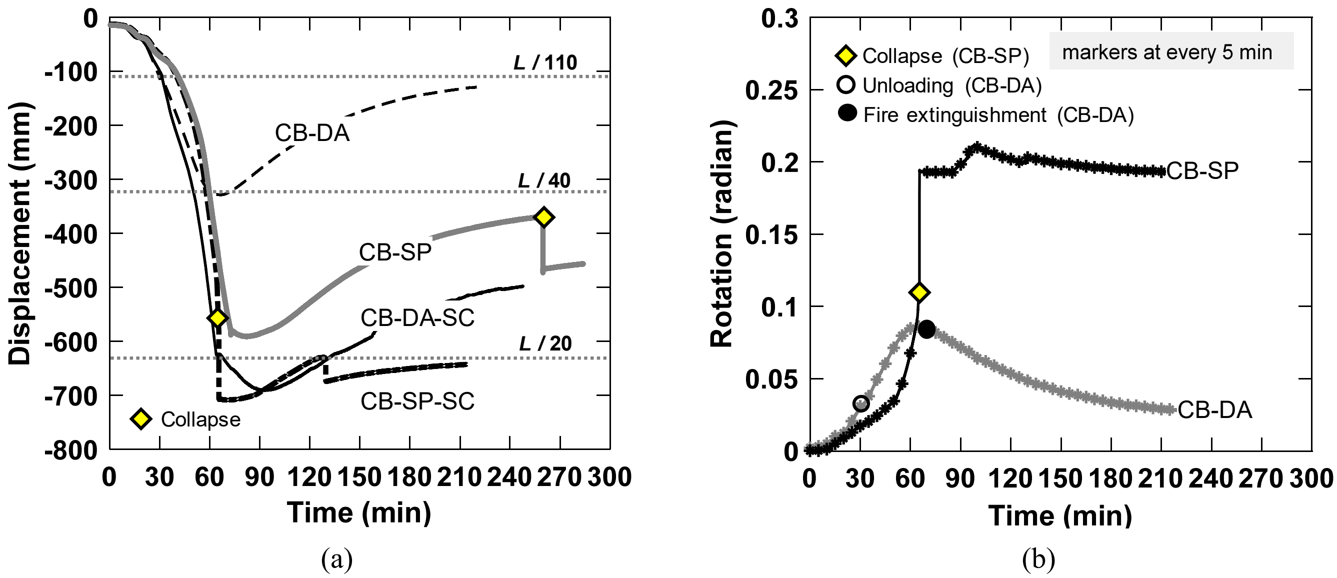

Fig. 7. (a) Vertical displacements of all four specimens measured near midspan and (b) measured slab end rotations of CB-DA and CB-SP

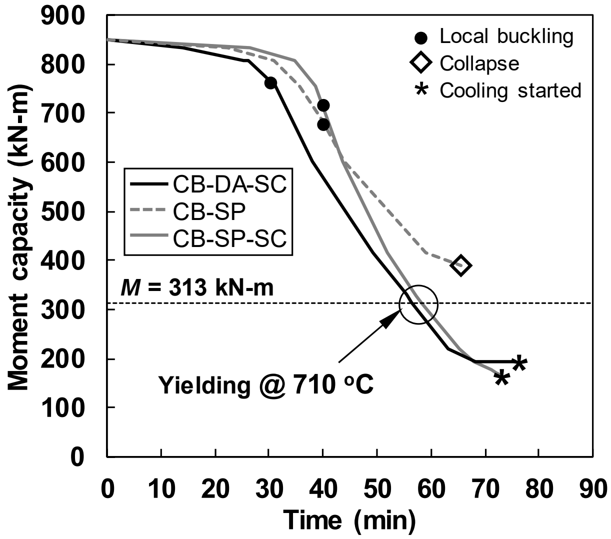

(a)

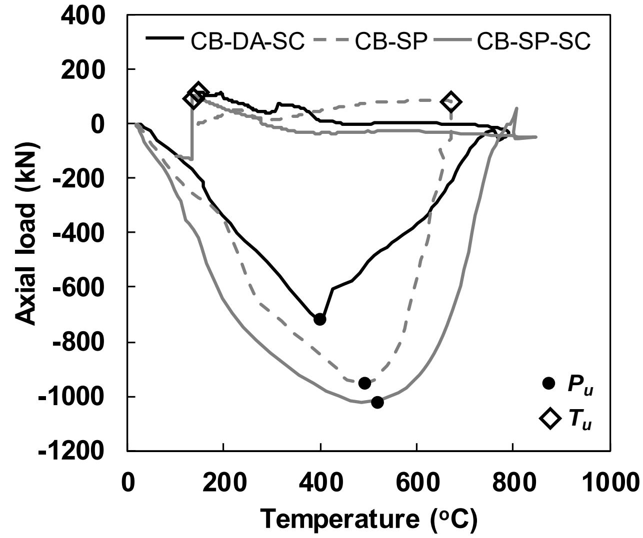

(b)

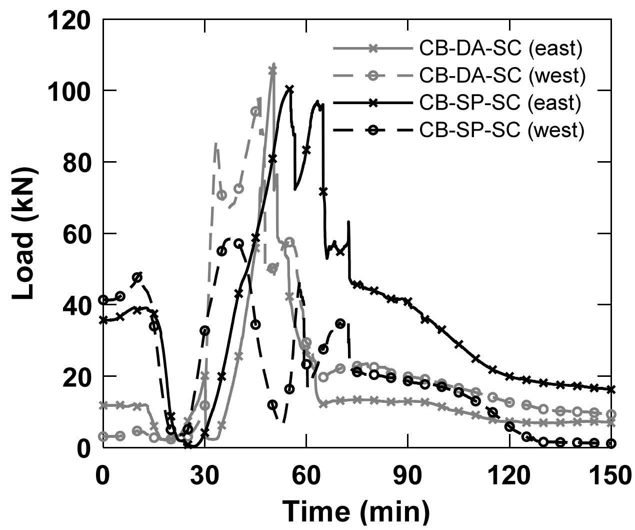

(c)

Fig. 8. (a) Axial loads at beam ends; (b) temperature-dependent moment capacity; and (c) total tensile loads on No.4 reinforcing bars at the east and west ends. P_u, T_u, and M_u indicate local buckling capacities, tensile capacities of connections, and applied moments at midspan, respectively.

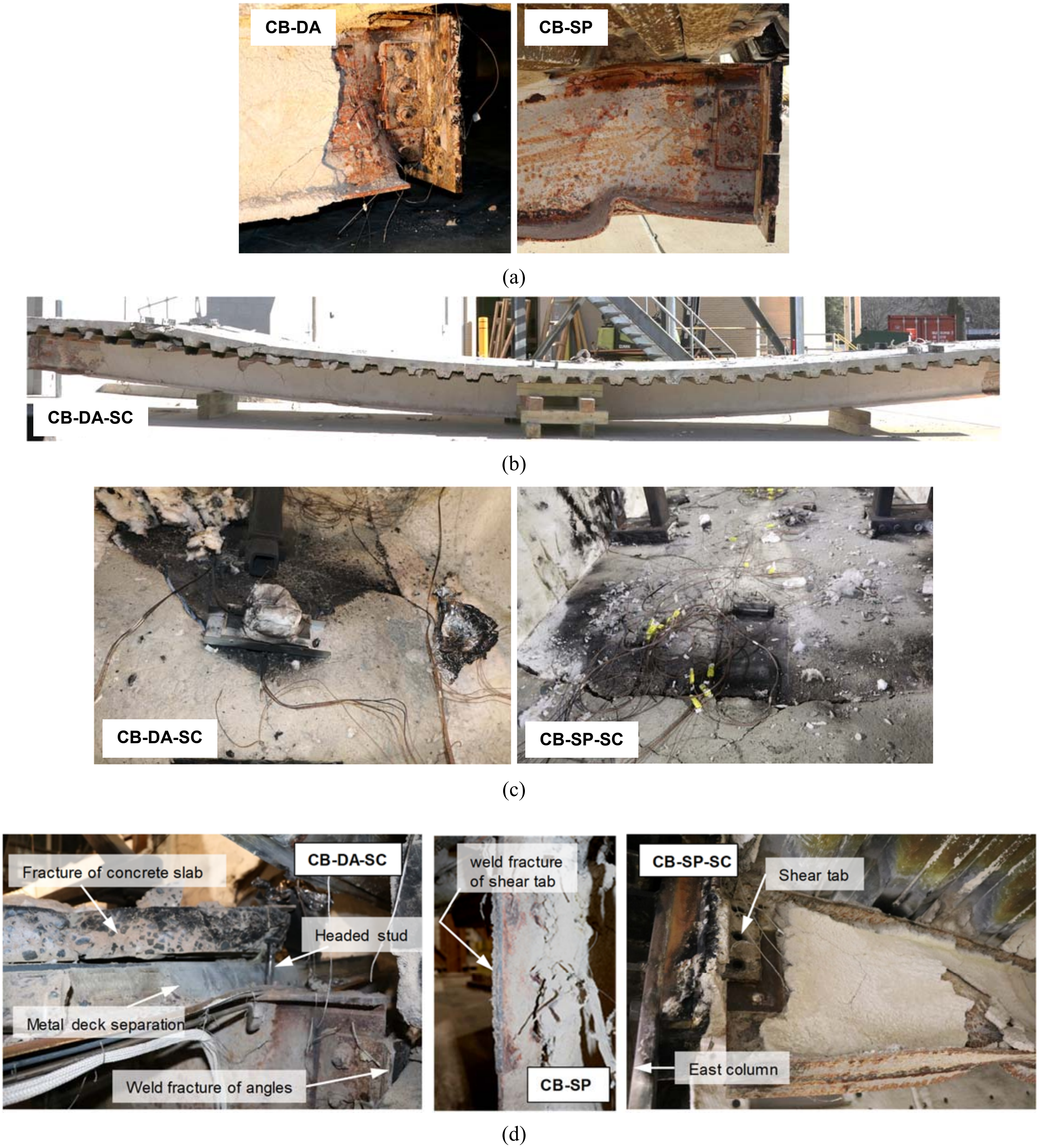

Fig. 9. Photographs of (a) locally bucked ends of CB-DA and CB-SP; (b) final deflected shape of CB-DA-SC; (c) concrete cracks of CB-DA-SC and CB-SP-SC near the west end; and (d) failure of the east connections of CB-DA-SC, CB-SP, and CB-SP-SC after cooling